Frontiers in Computing and Intelligent Systems
ISSN: 2832-6024 | Vol. 15, No. 2, 2026

Near-Infrared Photodetection Enabled by Interface-Purified $WS_2/MoTe_2$ Heterojunctions via Dual hBN Encapsulation

Chunli Zhou, Jieyu Dai, Huafeng Dong *

School of Physics and Optoelectronic Engineering, Guangdong University of Technology, Guangzhou, Guangdong, China
*** Corresponding author:** Huafeng Dong

Abstract: High-performance near-infrared photodetection is of great importance for applications in optical communication and imaging. Here, a vertically stacked $WS_2/MoTe_2$ van der Waals heterojunction with dual hBN encapsulation is constructed. Benefiting from interface purification and synergistic band structure modulation, the device exhibits significantly enhanced photoconversion efficiency and an extended spectral response range. A high responsivity of 13021 A W^{-1} and a detectivity of 5.39×10^{14} Jones are achieved at 405 nm. In the near-infrared region, responsivities of 586 A W^{-1} and 2292 A W^{-1} are obtained at 808 nm and 1064 nm, respectively, with a maximum detectivity of 9.49×10^{13} Jones. Stable time-response characteristics are maintained across all measured wavelengths. These results demonstrate that interfacially purified van der Waals heterostructures provide an effective strategy for high-performance two-dimensional near-infrared photodetectors.

Keywords: $WS_2/MoTe_2$ Heterojunction; Near-infrared Photodetection; Interface Engineering.

1. Introduction

Near-infrared photodetection holds significant application value in fields such as optical communications, laser ranging, and bioimaging [1-3]. Current mainstream near-infrared detection materials such as HgCdTe and InGaAs have achieved high performance in practical applications. However, their epitaxial growth processes are complex and costly, and they face certain limitations in flexible integration and low-dimensional device platforms [1-3]. Therefore, exploring alternative material systems that are compatible with novel integrated architectures and exhibit outstanding optoelectronic performance has become a significant research direction.

Two-dimensional materials offer a crucial platform for next-generation photodetectors due to their atomic-scale thickness, strong light-matter interactions, and absence of lattice mismatch [4-6]. Graphene was first utilized to achieve ultrafast broadband detection [7], and combined with quantum dots to realize high-gain phototransistors [8]. Subsequently, transition metal dichalcogenides (TMDs) have garnered significant attention due to their tunable bandgaps and exceptional electrical properties [9]. Monolayer MoS_2 has been demonstrated to be a direct-bandgap semiconductor [10-11] and has enabled high-sensitivity photodetection [12-13]. Furthermore, graphene/TMD hybrid structures also exhibit enhanced optoelectronic conversion capabilities [14-15].

However, the intrinsic optical absorption of most TMD materials is primarily confined to the visible spectral region [10-11]. To overcome this limitation, narrow-bandgap two-dimensional materials have been introduced into near-infrared detection research. For example, black phosphorus devices have achieved waveguide-integrated near-infrared detection [16] and demonstrated broad spectral response capabilities [17]. $MoTe_2$ has been extensively investigated due to its narrow bandgap and near-infrared optical absorption characteristics [18].

Although narrow-bandgap materials can broaden the absorption range, single-layer two-dimensional devices are often affected by interface states and environmental adsorption, leading to hysteresis and stability issues [19]. Constructing van der Waals heterojunctions enhances carrier separation through band alignment and built-in electric fields, serving as an effective approach to improve optoelectronic performance [20-22]. For example, MoS_2/WSe_2 and MoS_2/WS_2 heterostructures have demonstrated tunable photovoltaic effects and rapid charge transfer behavior [23-24]. The interlayer exciton phenomenon further demonstrates the significant impact of interfacial coupling on carrier dynamics [25].

Meanwhile, surface quality significantly impacts the performance of heterojunctions. Due to its atomic-level flatness and low trap density, hBN is widely utilized as a high-quality substrate and encapsulation material for two-dimensional materials [26]. hBN encapsulation can significantly enhance device stability and mobility [27], and further improve charge injection efficiency [28]. Additionally, clean interfaces can enhance the uniformity of interlayer coupling [29-30]. High-quality van der Waals heterointerfaces can also achieve enhanced optoelectronic and electroluminescent properties [31].

Based on the aforementioned research progress, this work constructed a fully encapsulated $WS_2/MoTe_2$ van der Waals heterojunction with dual hBN layers. Through interface purification and synergistic band structure regulation, it achieved significantly enhanced photocurrent output and near-infrared response capability. The device exhibits a responsivity of 13021 A W^{-1} and a detectivity of 5.39×10^{14} Jones at 405 nm, with responsivities of 586 A W^{-1} and 2292 A W^{-1} at 808 nm and 1064 nm, respectively, enabling broad-spectrum detection from visible light to wavelengths exceeding 1064 nm. This demonstrates that interface-engineered van der Waals heterostructures provide an effective design strategy for high-performance near-infrared two-dimensional photodetection.

2. Result and Discussion

To achieve stable and efficient near-infrared photodetection, we fabricated a $WS_2/MoTe_2$ vertical van der Waals heterojunction and fully encapsulated it with top and bottom layers of hBN, as shown in Figure 1. Figures 1a–c show the layered crystal structures of WS_2, $MoTe_2$, and hBN, respectively. WS_2 belongs to the class of wide-bandgap transition metal dichalcogenide (TMD) materials, exhibiting high environmental stability and electron mobility. $MoTe_2$ possesses a relatively narrow bandgap, with its absorption edge extending into the near-infrared region. Constructing these two materials into a vertical heterostructure forms a type-II band alignment, generating an intrinsic electric field at the interface, facilitating the spatial separation of photo-generated electrons and holes. However, conventional TMD heterojunctions typically come into direct contact with SiO_2 substrates and air. Residual interface materials, adsorbed surface molecules, and substrate charge fluctuations introduce a large number of trap states at the interface, thereby limiting the device's response speed and detection sensitivity. To address these issues, we introduce a dual hBN encapsulation structure. Figure 1d illustrates the complete device assembly process and the final structural schematic. The bottom hBN layer provides an atomically flat interface free of dangling bonds, while the top hBN layer effectively shields against water molecules in the air. This interface purification strategy stabilizes the potential barrier at the $WS_2/MoTe_2$ junction and ensures a more uniform potential distribution. Consequently, the built-in electric field enhances the separation efficiency of photo-generated carriers.

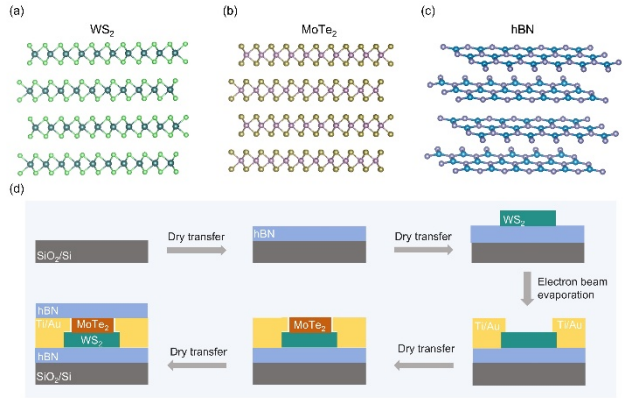


Fig 1. Schematic diagram of the structural design and fabrication process for the double hBN-encapsulated $WS_2/MoTe_2$ heterojunction. (a–c) Schematic diagrams of the crystal structures of multilayer WS_2, $MoTe_2$, and hBN. (d) Schematic diagram of the device fabrication process.

As shown in Figure 2a, WS_2 and $MoTe_2$ form a vertically stacked region between the electrodes and are fully encapsulated by the top layer of hBN. This structure generates a stable built-in electric field at the interface, providing the driving force for photogenerated carrier separation. Figures 2b–f display the I–V characteristics of the heterojunction under illumination at different wavelengths. Within the visible light range of 405–635 nm, the devices exhibit a significant increase in current under illumination, with a pronounced enhancement trend as incident power increases. This indicates that photo-generated carriers can be effectively separated and collected. As the incident wavelength increased to 808 nm and 1064 nm, the devices continued to exhibit a distinct and stable optical response. Particularly at 1064 nm, the photocurrent showed a significant enhancement compared to the dark state, demonstrating that this heterostructure successfully achieved effective detection in the near-infrared band. This broad spectral response capability stems from the bandgap alignment formed at the $WS_2/MoTe_2$ interface. The narrow-bandgap $MoTe_2$ absorbs low-energy photons, while the built-in electric field within the interface drives the spatial separation of photo-generated electrons and holes, reducing recombination probability and thereby significantly enhancing photocurrent output.

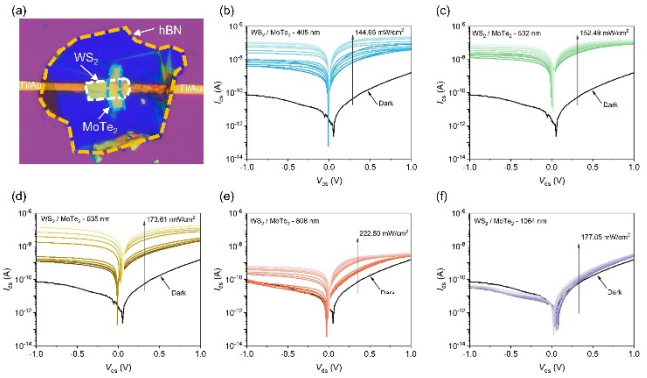


Fig 2. Broad-spectrum photoresponse characteristics of $WS_2/MoTe_2$ heterojunctions encapsulated with double-layer hBN. (a) Optical microscopic image of the heterojunction devices, the white scale bar corresponds to 20 μm. (b–f) I_{ds}–V_{ds} characteristic curves of the devices under laser irradiation at 405, 532, 635, 808, and 1064 nm.

To demonstrate the impact of heterostructures on optoelectronic performance, we fabricated bare WS_2 devices as controls and characterized their properties, as shown in Figure 3. Under visible light irradiation, bare WS_2 devices exhibit a certain degree of photoresponse, but the enhancement in photocurrent is significantly lower than that of heterojunction devices. The response is primarily concentrated in the 405–635 nm wavelength range and does not demonstrate effective detection capabilities for longer wavelengths. In contrast, the $WS_2/MoTe_2$ heterostructure employs an interface bandgapping mechanism to achieve spatial separation, significantly enhancing photocurrent output while extending spectral response into the near-infrared region.

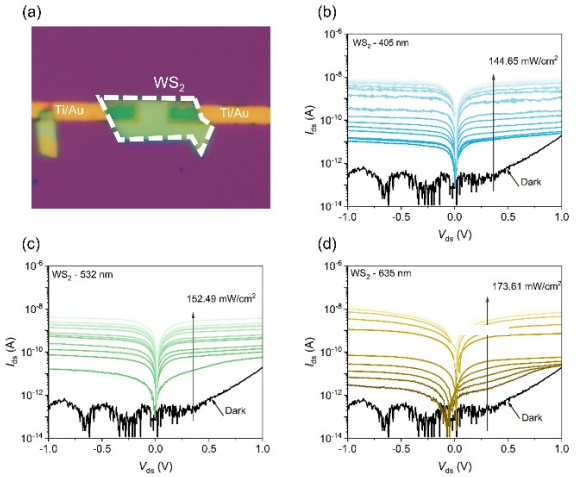


Fig 3. Photoelectric response characteristics of bare WS_2 devices. (a) Optical microscope image of the bare WS_2 devices, the white scale bar corresponds to 20 μm. (b–d) I_{ds}–V_{ds} curves of the devices under 405, 532, and 635 nm laser irradiation.

This demonstrates the pivotal role of interface engineering in enhancing the performance of two-dimensional optoelectronic devices.

To further evaluate the dynamic performance of heterojunction devices under modulated light conditions, we conducted time response tests across the 405–1310 nm wavelength range. The results are shown in Figures 4 and 5. Under 405, 532, and 635 nm conditions, the device's photocurrent rapidly establishes and decays under optical switching, with rise and fall times both in the millisecond range.

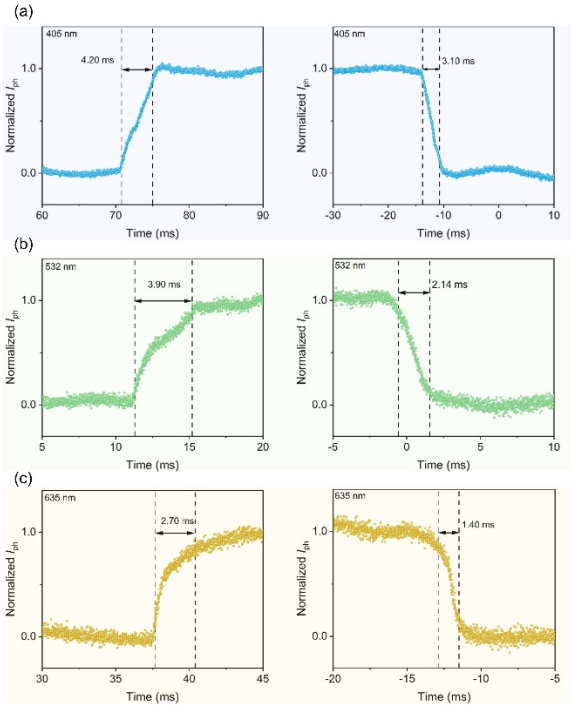


Fig 4. Time-response characteristics of $WS_2/MoTe_2$ heterojunctions in the visible light spectrum. (a-c) Normalized photocurrent-time curves of heterojunction devices under modulated illumination at 405, 532, and 635 nm, showing both the rise and decay processes for each wavelength.

At 808 nm, millisecond-level response is maintained, indicating the device's stable response to periodic optical signals across the visible-to-near-infrared transition region. When the wavelength increases to 1064 nm, a distinct modulation response remains observable, though the response time extends to tens of milliseconds. At 1310 nm, discernible switching signals can still be detected. Combined with the aforementioned photocurrent enhancement results, it can be observed that the $WS_2/MoTe_2$ heterojunction not only achieves an expanded spectral response range but also maintains stable time response capabilities under modulated light conditions.

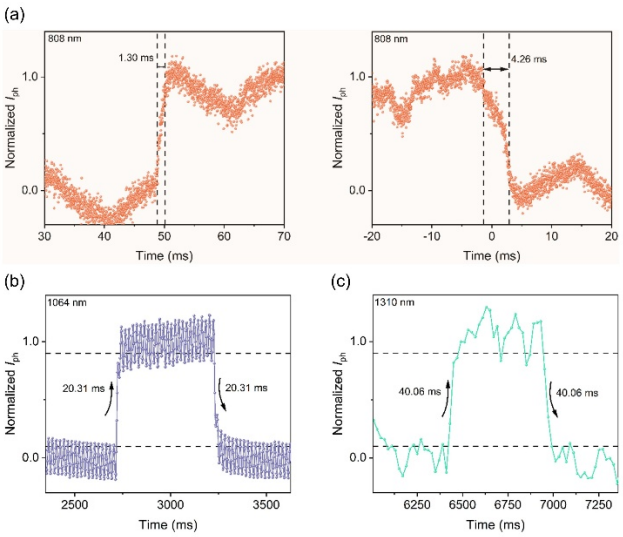


Fig 5. Time response characteristics of $WS_2/MoTe_2$ heterojunctions in the near-infrared wavelength range.

To further quantitatively evaluate the enhancement of optoelectronic performance by the heterostructure, we compared the responsivity (R) and detectivity (D*) of the heterojunction devices with that of the bare WS_2 devices, as shown in Figures 6 and 7. Under 405 nm illumination, the $WS_2/MoTe_2$ heterojunction exhibits significantly enhanced photoconversion capabilities. At low power densities, its responsivity reaches up to 13021 A W^{-1}, with a detectivity of 5.39×10^{14} Jones. In contrast, under identical testing conditions, the bare WS_2 devices exhibited a responsivity of only 0.802 A W^{-1} and a detectivity of 3.01×10^{11} Jones. The difference in responsivity and detectivity spans several orders of magnitude, demonstrating the significant enhancement of photoconversion efficiency through interfacial synergy. At wavelengths of 532 nm and 635 nm, the heterojunction devices maintain high R and D* values, whereas the bare WS_2 devices exhibit only limited performance enhancement, with effective response limited to wavelengths up to 635 nm.

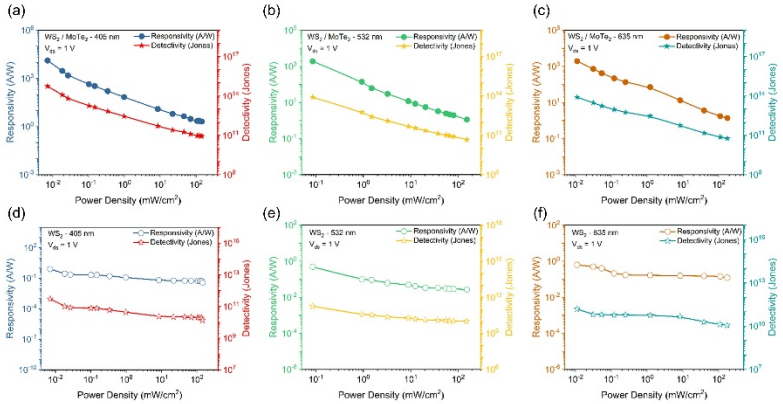


Fig 6. Comparison of responsivity and detectivity in the visible light spectrum between heterojunction and bare WS_2 devices. (a–c) Response (R) and Detectivity (D*) of $WS_2/MoTe_2$ heterojunctions versus incident power density at 405, 532, and 635 nm. (d–f) Response (R) and Detectivity (D*) of bare WS_2 devices versus incident power density at 405, 532, and 635 nm

More importantly, the heterojunction devices continue to exhibit outstanding performance in the near-infrared wavelength range. As shown in Figure 7, under 808 nm conditions, the responsivity reaches 586 A W^{-1}, with a detectivity of 2.43 × 10^{13} Jones. At 1064 nm, the responsivity further increases to 2292 A W^{-1}, corresponding to a detectivity of 9.49 × 10^{13} Jones. The WS_2/$MoTe_2$ heterostructure achieves broad spectral expansion from visible to near-infrared light while maintaining stable time response, demonstrating enhanced photoconversion performance across the entire tested wavelength range.

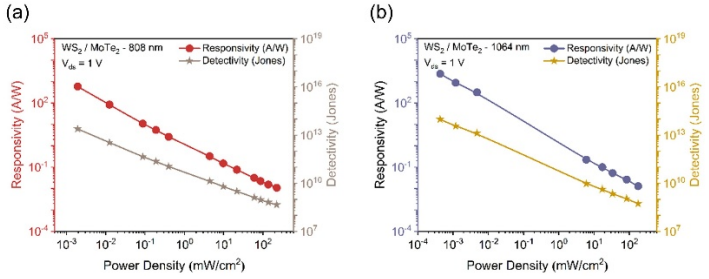


Fig 7. Response and detection performance of heterojunction devices in the near-infrared wavelength range. (a) Relationship between responsivity and detectivity versus power at 808 nm. (b) Variation curves of responsivity and detectivity at 1064 nm

3. Conclusion

This work constructs a vertically stacked WS_2/$MoTe_2$ van der Waals heterojunction photodetector with dual hBN encapsulation, achieving broadband spectral response from the visible to near-infrared region. Through interfacial synergy, the heterojunction device exhibits a maximum responsivity of 13021 A W^{-1} and a detectivity of 5.39 × 10^{14} Jones at 405 nm, significantly outperforming bare WS_2 devices. In the near-infrared region, high responsivities of 586 A W^{-1} and 2292 A W^{-1} are obtained at 808 nm and 1064 nm, respectively, with a detectivity of 9.49 × 10^{13} Jones at 1064 nm. Time-response measurements demonstrate stable modulation behavior across the visible-to-near-infrared spectrum, with response times ranging from milliseconds to tens of milliseconds. Compared with bare devices, the heterostructure not only markedly enhances photocurrent amplitude but also effectively broadens the spectral response range. Overall, the dual hBN-encapsulated WS_2/$MoTe_2$ heterojunction achieves systematic enhancement of optoelectronic performance via interface engineering, providing a viable structural strategy for high-performance near-infrared photodetection based on two-dimensional materials.

4. Experimental Section

Devices Fabrication: Heterojunction devices were fabricated on p+-type silicon/silicon dioxide substrates (500 μm/300 nm). Electrode patterns (channel length 20 μm) were defined via standard UV photolithography. Subsequently, Ti/Au films (5/50 nm) were deposited by electron beam evaporation, followed by a lift-off process to form contact electrodes. Using a micromanipulation system (Shanghai Anwei Technology Co., Ltd), few-layer hexagonal boron nitride (hBN) flakes mechanically exfoliated from single crystals (Taizhou SUNANO New Energy Co., Ltd) were dry-transferred between the Ti/Au electrodes, avoiding direct contact with the metal contact points during handling. The mechanically exfoliated WS_2 flakes were then transferred onto the hBN layer, ensuring complete coverage of the bottom hBN layer and electrical connection to the adjacent Ti/Au electrodes. Subsequently, exfoliated $MoTe_2$ flakes were precisely aligned and transferred onto the WS_2 channel region, avoiding contact with the electrodes. Finally, the device was encapsulated using mechanically exfoliated few-layer hBN flakes via dry transfer technology, completing the vertical van der Waals heterojunction structure.

Devices Measurements: The morphology of the fabricated devices was inspected using an optical microscope (Motic, BA310Met). All electrical and optoelectronic measurements were performed in ambient conditions using a probe station coupled with a source meter (Keithley, 2636B). The incident power was calibrated using a silicon photodiode (Thorlabs, S120VC). For wavelength-dependent measurements, monochromatic lasers at 405, 532, 635, 808, 1064 and 1310 nm were used as light sources. The laser spot size (0.36 cm^2) was significantly larger than the active device area (95 μm^2) to ensure uniform illumination. Temporal photoresponse measurements were conducted by modulating the laser with a function generator and recording the photocurrent with a digital oscilloscope (Tektronix, DPO4102B).

Acknowledgments

The authors gratefully acknowledge the Instrumental Analysis Center of Guangdong University of Technology, Guangzhou, China, for providing experimental facilities and technical support.

References

[1] A. Rogalski, *Infrared detectors: status and trends.* Prog. Quantum Electron., 2003. **27**(2-3): p. 59-210.

[2] A. Rogalski, *HgCdTe infrared detector material: history, status and outlook.* Rep. Prog. Phys., 2005. **68**(10): p. 2267-2336.

[3] A. Rogalski, P. Martyniuk, M. Kopytko, *InAs/GaSb type-II superlattice infrared detectors: Future prospect.* Appl. Phys. Rev., 2017. **4**(3).

[4] A.K. Geim, I.V. Grigorieva, *Van der Waals heterostructures.* Nature, 2013. **499**(7459): p. 419-425.

[5] K.S. Novoselov, A.K. Geim, S.V. Morozov, et al., *Electric field effect in atomically thin carbon films.* Science, 2004. **306**(5696): p. 666-669.

[6] M. Long, P. Wang, H. Fang, W. Hu, *Progress, challenges, and opportunities for 2D material based photodetectors.* Adv. Funct. Mater., 2019. **29**(19): p. 1803807.

[7] F. Xia, T. Mueller, Y.-m. Lin, A. Valdes-Garcia, P. Avouris, *Ultrafast graphene photodetector.* Nat. Nanotechnol., 2009. **4**(12): p. 839-843.

[8] G. Konstantatos, M. Badioli, L. Gaudreau, et al., *Hybrid graphene–quantum dot phototransistors with ultrahigh gain.* Nat. Nanotechnol., 2012. **7**(6): p. 363-368.

[9] K.F. Mak, J. Shan, *Semiconductor moiré materials.* Nat. Nanotechnol., 2022. **17**(7): p. 686-695.

[10] A. Splendiani, L. Sun, Y. Zhang, et al., *Emerging photoluminescence in monolayer MoS_2.* Nano Lett., 2010. **10** (4): p. 1271-1275.

[11] K.F. Mak, C. Lee, J. Hone, J. Shan, T.F. Heinz, *Atomically thin MoS_2: a new direct-gap semiconductor.* Phys. Rev. Lett., 2010. **105**(13): p. 136805.

[12] O. Lopez-Sanchez, D. Lembke, M. Kayci, A. Radenovic, A. Kis, *Ultrasensitive photodetectors based on monolayer MoS_2.* Nat. Nanotechnol., 2013. **8**(7): p. 497-501.

[13] W. Zhang, J.K. Huang, C.H. Chen, et al., *High-gain phototransistors based on a CVD MoS_2 monolayer.* Adv. Mater., 2013. **25**(25): p. 3456-3461.

[14] K. Roy, M. Padmanabhan, S. Goswami, et al., *Graphene–MoS_2 hybrid structures for multifunctional photoresponsive memory devices.* Nat. Nanotechnol., 2013. **8**(11): p. 826-830.

[15] F.H. Koppens, T. Mueller, P. Avouris, et al., *Photodetectors based on graphene, other two-dimensional materials and hybrid systems.* Nat. Nanotechnol., 2014. **9**(10): p. 780-793.

[16] N. Youngblood, C. Chen, S.J. Koester, M. Li, *Waveguide-integrated black phosphorus photodetector with high responsivity and low dark current.* Nat. Photonics, 2015. **9**(4): p. 247-252.

[17] M. Buscema, D.J. Groenendijk, S.I. Blanter, et al., *Fast and broadband photoresponse of few-layer black phosphorus field-effect transistors.* Nano Lett., 2014. **14**(6): p. 3347-3352.

[18] C. Ruppert, B. Aslan, T.F. Heinz, *Optical properties and band gap of single-and few-layer $MoTe_2$ crystals.* Nano Lett., 2014. **14**(11): p. 6231-6236.

[19] D.J. Late, B. Liu, H.R. Matte, V.P. Dravid, C. Rao, *Hysteresis in single-layer MoS_2 field effect transistors.* ACS Nano, 2012. **6**(6): p. 5635-5641.

[20] M.M. Furchi, A. Pospischil, F. Libisch, J. Burgdorfer, T. Mueller, *Photovoltaic effect in an electrically tunable van der Waals heterojunction.* Nano Lett., 2014. **14**(8): p. 4785-4791.

[21] C.-H. Lee, G.-H. Lee, A.M. Van Der Zande, et al., *Atomically thin p–n junctions with van der Waals heterointerfaces.* Nat. Nanotechnol., 2014. **9**(9): p. 676-681.

[22] A. Pospischil, M.M. Furchi, T. Mueller, *Solar-energy conversion and light emission in an atomic monolayer p–n diode.* Nat. Nanotechnol., 2014. **9**(4): p. 257-261.

[23] R. Cheng, D. Li, H. Zhou, et al., *Electroluminescence and photocurrent generation from atomically sharp WSe_2/MoS_2 heterojunction p–n diodes.* Nano Lett., 2014. **14**(10): p. 5590-5597.

[24] X. Hong, J. Kim, S.-F. Shi, et al., *Ultrafast charge transfer in atomically thin MoS_2/WS_2 heterostructures.* Nat. Nanotechnol., 2014. **9**(9): p. 682-686.

[25] P. Rivera, J.R. Schaibley, A.M. Jones, et al., *Observation of long-lived interlayer excitons in monolayer $MoSe_2$–WSe_2 heterostructures.* Nat. Commun., 2015. **6**(1): p. 6242.

[26] C.R. Dean, A.F. Young, I. Meric, et al., *Boron nitride substrates for high-quality graphene electronics.* Nat. Nanotechnol., 2010. **5**(10): p. 722-726.

[27] G.-H. Lee, X. Cui, Y.D. Kim, et al., *Highly stable, dual-gated MoS_2 transistors encapsulated by hexagonal boron nitride with gate-controllable contact, resistance, and threshold voltage.* ACS Nano, 2015. **9**(7): p. 7019-7026.

[28] L. Wang, I. Meric, P. Huang, et al., *One-dimensional electrical contact to a two-dimensional material.* Science, 2013. **342** (6158): p. 614-617.

[29] D.G. Purdie, N. Pugno, T. Taniguchi, et al., *Cleaning interfaces in layered materials heterostructures.* Nat. Commun., 2018. **9**(1): p. 5387.

[30] M.R. Rosenberger, H.-J. Chuang, M. Phillips, et al., *Twist angle-dependent atomic reconstruction and moiré patterns in transition metal dichalcogenide heterostructures.* ACS Nano, 2020. **14**(4): p. 4550-4558.

[31] F. Withers, O. Del Pozo-Zamudio, A. Mishchenko, et al., *Light-emitting diodes by band-structure engineering in van der Waals heterostructures.* Nat. Mater., 2015. **14**(3): p. 301-306.